Multifunctional Organosulfonate Anions Self-Assembled with Organic Cations by Charge-Assisted Hydrogen Bonds and the Cooperation of Water

CRYSTAL GROWTH & DESIGN

Article

pubs.acs.org/crystal

Multifunctional Organosulfonate Anions Self-Assembled with Organic Cations by Charge-Assisted Hydrogen Bonds and the Cooperation of Water

Guolong Xing,[†,‡] Irene Bassanetti,[‡] Teng Ben,[*,†] Silvia Bracco,[‡] Piero Sozzani,[‡] Luciano Marchio,[*,§] and Angiolina Comotti[*,‡]

[†]Department of Chemistry, Jilin University, 130012 Changchun, China

[‡]Department of Materials Science, University of Milano Bicocca, Via R. Cozzi 55, 20125 Milan, Italy

[§]SCVSA Department, University of Parma, 43124, Parma, Italy

Supporting Information

ABSTRACT: The present study focuses on the assembly of organo-cations with organo-anions in water. The anions, characterized by symmetric moieties (carbon-, adamantane-, or calixarene-based) functionalized with directional hydrogen bond (HB) acceptor functions (tetra-sulfonate moieties), are combined with planar guanidinium or terephtalimidamide cations as hydrogen bond donors, the purpose being to integrate water molecules into the lattice. The imbalance between the charge on the two components, and the considerable number of HB donor and acceptor sites, promotes the insertion of water into the structures. In the reported structures, a part of the water molecules serves as a structural linker between the anions and cations, while the remaining molecules cluster into channels and cavities in a loose association with the supramolecular matrix framework.

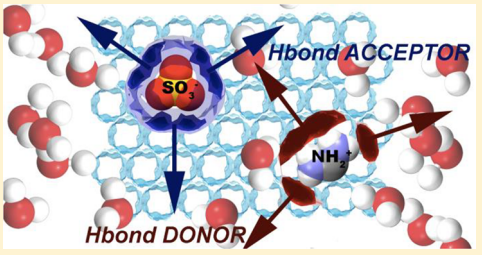

INTRODUCTION

Fully organic ionic solids integrate electrostatic interactions with hydrogen bonding (HB),[1−5] weak interactions,[6,7] and shape factors to sustain crystal assemblies.[8,9] Thus, organic molecules of opposite charge promote the formation of supramolecular buildings where electroneutrality and stoichiometry are dominant structure-directing features.[10−13] The self-assembly of charged organic molecules[14−16] for the formation of crystalline architecture is based on the coupling of complementary charged functionalities,[17,18] such as carboxylate[19−24] and sulfonate anions[25−28] with ammonium,[29] or sulfonate[30] with other organo-cations. In this context, a wide range of two-component supramolecular structures[25,28,31,32] has been fabricated, especially during the past few years. The construction of complex crystal architectures implies both the multiplication of organic functionalities on the same molecule and control over their space orientation.[33−35] The degree of complexity increases progressively with the use of multidentate molecular struts combined with the planar and three-dimensional (3D) geometries of the components.

The probability of hydrate formation is enhanced by introducing multiple functionalities, especially when there is an uneven number of HB donors and acceptors, as well as increased molecule complexity, which promotes ineffective packing.[36−38] Moreover, the ionic nature of organic moieties makes them compatible with aqueous media, feeding the structure with water as an additional and constructive building element.[30,38−41] From the applicative point of view, hydrate formation is a central issue in pharmaceutical applications,[42,43] providing enhanced solubility, stability, and response to the environment compared to the anhydrous precursors.

The water molecules contained in the lattice can usually be divided into two categories with two different roles: one is structural, the water molecules serving to sustain the lattice architecture, and the second relates to the occupation of cavities formed by hydrogen bonded components.[19] Accordingly, channels, pores, and discrete pockets contain water in clusters of different sizes.[44] In the present work, while investigating the aggregation of organic molecules bearing multiple charges, we found interesting hydrated structures and discriminated between hard and soft host/water interactions. We were intrigued by the 3D geometries of the building blocks and explored a few polyfunctional organosulfonates self-assembled with mono- or organo-dications (Scheme 1). Our investigation encompassed tetrahedral and conical orientation of the sulfonate groups. We obtained six charge-assisted hydrogen bonded organic frameworks, which were studied by spectroscopic techniques (^{1}H NMR, IR) and thermal methods (thermogravimetric analysis (TGA) and differential scanning calorimetry (DSC)). Crystals suitable for conventional and synchrotron radiation X-ray diffraction characterization were grown from aqueous media, and their single crystal X-ray structures were determined. The comparison of the structural features of these charge-assisted systems allowed us to highlight

Received: November 3, 2017
Revised: February 19, 2018
Published: February 26, 2018

DOI: 10.1021/acs.cgd.7b01538
Cryst. Growth Des. XXXX, XXX, XXX−XXX

Scheme 1. Schematic Representation of Anionic (Red)/Cationic (Blue) Components Used To Synthesize Charged Organic-Molecule Suprastructures

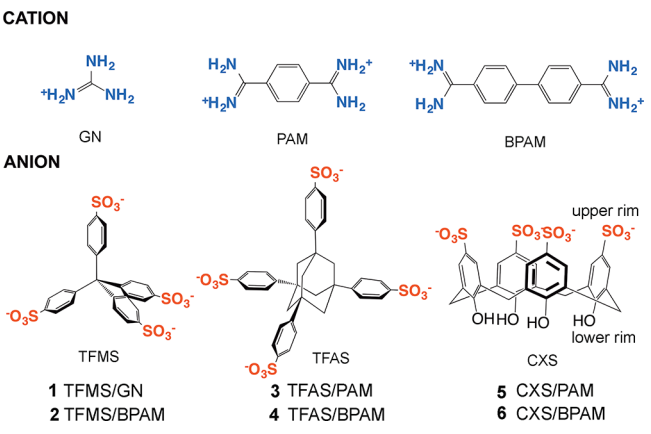

the role of multidentate charged molecules in the formation of structures, and the tendency to integrate matrix and water molecules into crystal architectures.

EXPERIMENTAL SECTION

4,4′,4″,4‴-Methanetetrayltetrabenzenesulfonic acid (H_4TFMS), 4,4′,4″,4‴-(adamantane-1,3,5,7-tetrayl)tetrabenzenesulfonic acid (H_4TFAS), terephtalimidamide hydrochloride (PAM·HCl), and [1,1′-biphenyl]-4,4′-bis(carboximidamide) dihydrochloride (BPAM·2HCl) were prepared as previously described, or as reported in the literature, and used in their protonated forms.[45−48] Guanidinium hydrochloride (GN·HCl), 4-sulfocalix[4]arene (H_4CXS), and all solvents used for synthesis, and crystallization were commercially available and used as received. NMR spectra were recorded on Bruker AVANCE III (400 MHz). Chemical shifts (δ) for ^{1}H spectra were referenced using internal solvent resonances and are reported relative to tetramethylsilane (TMS). According to ^{1}H NMR, the ratio between cationic and anionic components is easily evaluated, and the amount of water in the molecular adduct is calculated by subtracting the one found in the deuterated solvent considered as blank. Fourier transform infrared (FT-IR) spectra (4000−700 cm^{-1}) were recorded on a Nicolet Nexus spectrophotometer equipped with a Smart Orbit HATR accessory (diamond crystal). DSC data were recorded on a Mettler Toledo Stare DSC1 analysis system equipped with low temperature apparatus. The experiments were run under nitrogen atmosphere in standard 40 μL Al pans. The DSC analyses were performed from 25 to 200 °C (10 °C/min) to study the transformation related to water and solvent molecule loss, and to compare them to crystal structure information. TGA was collected on a PerkinElmer instrument (samples mass approximately 5−10 mg) from 25 to 400 °C under nitrogen flow (80 mL/min). See Supporting Information for details on ^{1}H NMR and IR spectroscopy, TGA, and DSC analysis.

Synthesis. *Synthesis of* ***1****.* H_4TFMS (27.4 mg, 0.032 mmol) dissolved in 0.5 mL of MeOH was gently added to a solution of GN·HCl (12.2 mg, 0.128 mmol) in 0.5 mL of MeOH in an open vial. After 24 h, white crystals suitable for X-ray data collection were obtained from the solution, corresponding to $(GN)_4(TFMS)\cdot 8H_2O$ (**1**). The solid was filtered out and vacuum-dried (17 mg, yield 62%).

Synthesis of ***2****.* H_4TFMS (20.5 mg, 0.024 mmol) was dissolved in a mixture of 0.1 mL of NaOH (1 M), 0.9 mL of water, and 3.0 mL of THF. To the mixture, BPAM·2HCl (14.9 mg, 0.048 mmol) dissolved in 1 mL of water and 2.5 mL of THF was added. After 24 h, light yellow crystals suitable for X-ray data collection were obtained from the solution, corresponding to $(BPAM)_2(TFMS)\cdot 13H_2O$ (**2**). The solid was filtered out and vacuum-dried (17 mg, yield 67%).

Synthesis of ***3****.* H_4TFAS (18.4 mg, 0.024 mmol) was dissolved in a mixture of 0.1 mL of NaOH (1 M), 0.9 mL of water, and 1.0 mL of EtOH. To the mixture, PAM·HCl (11.3 mg, 0.048 mmol) dissolved in 1.0 mL of water and 1.0 mL of EtOH was added. After 24 h, white crystals suitable for X-ray data collection were obtained from the solution, corresponding to $(PAM)_2(TFAS)\cdot 9H_2O$ (**3**). The solid was filtered out and vacuum-dried (16 mg, yield 63%).

Synthesis of ***4****.* H_4TFAS (9.2 mg, 0.012 mmol) was dissolved in a mixture of 0.05 mL of NaOH (1 M), 0.45 mL of water, and 2.0 mL of MeOH. To the mixture, BPAM·2HCl (7.5 mg, 0.024 mmol) dissolved in 0.5 mL of water and 1 mL of MeOH was added. After 24 h, white crystals suitable for X-ray data collection were obtained from the solution, corresponding to $(BPAM)_2(TFAS)\cdot 6.4H_2O\cdot 3.6MeOH$ (**4**). The solid was filtered out and vacuum-dried (12 mg, yield 78%).

Synthesis of ***5****.* H_4CXS (17.8 mg, 0.024 mmol), dissolved in 0.4 mL of water and 0.5 mL of MeOH, was gently added a solution of PAM·HCl (11.3 mg, 0.048 mmol) in 0.75 mL of water. After 24 h, white crystals suitable for X-ray data collection were obtained from solution, corresponding to $(PAM)_2CXS\cdot 4H_2O\cdot 0.5MeOH$ (**5**). The solid was filtered out and vacuum-dried (16 mg, yield 64%).

Synthesis of ***6****.* H_4CXS (8.9 mg, 0.012 mmol) dissolved in 0.5 mL of water and 1.0 mL of MeOH, was gently added to a solution of BPAM·2HCl (7.5 mg, 0.024 mmol) dissolved in 0.5 mL of water and 1 mL of MeOH. After 24 h, white crystals suitable for X-ray data collection were obtained from the solution, corresponding to $(BPAM)_2(CXS)\cdot 8H_2O\cdot 2CH_3OH$ (**6**). The solid was filtered out and vacuum-dried (12 mg, yield 79%).

X-ray Diffraction. A summary of data collection and structure refinement for **1**−**6** is reported in the Supporting Information Table S3. Single crystal data for **1**, **3**, and **6** were collected with a Bruker Smart APEXII at 200 K, whereas data for **2** were collected with a Bruker D8 PhotonII at 100 K, Mo Kα: λ = 0.71073 Å. The intensity data were integrated from several series of exposure frames (0.3° width) covering the sphere of reciprocal space.[49] Absorption correction was applied using the program SADABS.[50] The data collection for **4** and **5** was performed at the X-ray diffraction beamline (XRD1) of the Elettra Synchrotron, Trieste (Italy).[51] Data sets were collected at 100 K through the rotating crystal method. Completeness was obtained by merging two different data collections done on the same crystal, mounted with different orientations. Data were acquired using a monochromatic wavelength of 0.700 Å on a Pilatus 2M hybrid-pixel area detector. The diffraction data were indexed and integrated using XDS.[52] Scaling was done using CCP4-Aimless code.[53,54] The structures were solved by the dual space algorithm implemented in the SHELXT code.[55] Fourier analysis and refinement were performed by the full-matrix least-squares method based on F2 implemented in SHELXL-2014.[56] Graphical material was prepared with the Mercury 3.9 program.[57]

RESULTS AND DISCUSSION

Single crystal X-ray structures were determined for compounds **1**−**6**. In all systems, there can be identified three components, namely, organo-cation, organo-anion, and water/solvent molecules. The invariant feature of the organo-anion is the presence of four sulfonate groups that in TFMS and TFAS are oriented along the vertices of a tetrahedron, whereas in CXS they are oriented on the same side of the calixarene platform (Scheme 2). The sulfonate groups are expected to act as HB acceptors. As far as the organo-cations are concerned, the doubly charged PAM and BPAM exhibit the same number of HB donor groups (four NH_2 moieties), and their main difference derives from the additional torsional degree of freedom imparted by the biphenyl system in BPAM with respect to PAM. The smaller organo-cation of the series is GN, which exhibits three NH_2 groups arranged in a regular trigonal planar geometry bearing a single positive charge. The nature of the cation implies that six to eight HBs can be formed for GN and PAM/BPAM, respectively. In addition, the different symmetry of GN with respect to PAM/BPAM implies a different directionality of the HBs formed by these two groups

DOI: 10.1021/acs.cgd.7b01538
Cryst. Growth Des. XXXX, XXX, XXX−XXX

Scheme 2. (A) Geometrical Representation of the Cationic Components and (B) Full Interaction Maps[59] (the Interaction Experienced by HB Donors Is Depicted in Red). (C) Anionic Components and (D) Their Full Interaction Maps (the Interaction Experienced by HB Acceptors Is Depicted in Blue)

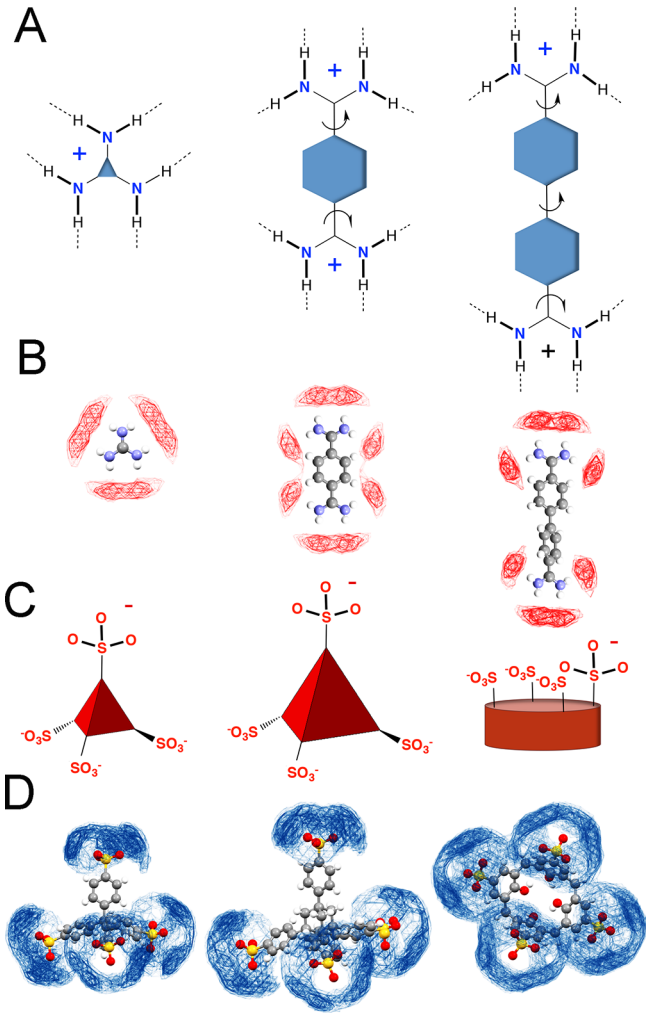

of cations, Scheme 2. In principle, there are nine potential structural outcomes when combining three cationic and three anionic components. Unfortunately, we could not recover suitable crystals from the TFMS/PAM and TFAS/GN mixtures; instead, the CXS/GN system has already been reported.[58]

As mentioned above, a third component was present in all the investigated systems, namely, water molecules or, to a minor extent, methanol molecules. Hence, besides the charge-assisted HBs detected for the cation and anion counterparts, HBs between the organic moieties and water molecules were observed. Not only was a large content of water found in the channels or pores of the structures, but it was found that water molecules were often active components in the construction of the supramolecular assembly bridging between organo-cation and organo-anions.

In compounds **1** and **2** tetrahedral TFMS was combined with two different organo-cations: GN and BPAM, Figures 1 and 2. Compounds **1** and **2** crystallize in the tetragonal space group $I4_1/a$ and in the monoclinic space group $C2/c$, respectively. The asymmetric unit of **1** consists of one phenyl-SO_3^- group,

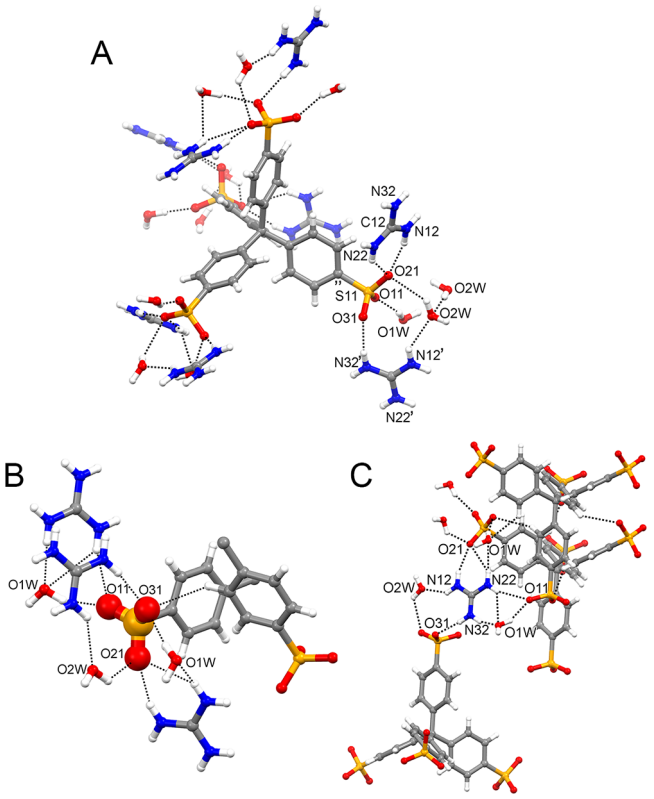

Figure 1. Molecular structure of **1**. The interactions exchanged by TFMS (A and B) and of GN (C). Symmetry codes: ′ = 5/4 − *y*; *x* − 1/4; *z* − 1/4, ′′ = 5/4 − *y*; *x* − 1/4; 3/4 + *z*.

one guanidinium cation, and two water molecules (O1w and O2w). Overall, the structural arrangement consists of four symmetry related GN interacting with a tetra-negatively charged TFMS and eight water molecules $(GN)_4(TFMS)\cdot 8H_2O$. The three structural components, namely, cation, anion and water molecules, interact extensively by means of HBs. Each oxygen atom of the SO_3^- group acts as an HB acceptor with water molecules and with the NHs of GN. The guanidinium cation acts as an HB donor with all its six hydrogen atoms (Figure 1C). It interacts with three oxygens of three symmetry related anions, and with three water molecules. The O2w molecule occupies a channel-like cavity, which is parallel to the *c* crystallographic axis, whereas O1w occupies one portion of space surrounded by cations and anions. The GN, TFMS, and H_2O ratio was also assessed by means of ^1H NMR on a sample of crystalline **1** dissolved in deuterated dimethyl sulfoxide (Supporting Information).

The stoichiometry of **2** comprises half TFMS moieties, a BPAM cation, and 6.5 water molecules of crystallization, $(BPAM)_2(TFMS)\cdot 13H_2O$. The BPAM cation exchanges several interactions with the surrounding anions and solvent molecules (Figure 2). The BPAM cation bridges the TFMS moieties by forming HBs with the sulfonate groups. Two NH_2 fragments on the opposite side of the BPAM unit form HBs, water molecules being located in channel-like cavities. According to the ^1H NMR spectrum recorded on a crystalline sample of **2**, the anion/cation/water ratio is approximately 1/2/9, whereas the structural refinement identified 13 water molecules in the channel-like cavities.

The crystal packing of compounds **1** and **2** shows interesting similarities (Figure 3). In fact, the three different architectural

DOI: 10.1021/acs.cgd.7b01538
Cryst. Growth Des. XXXX, XXX, XXX−XXX

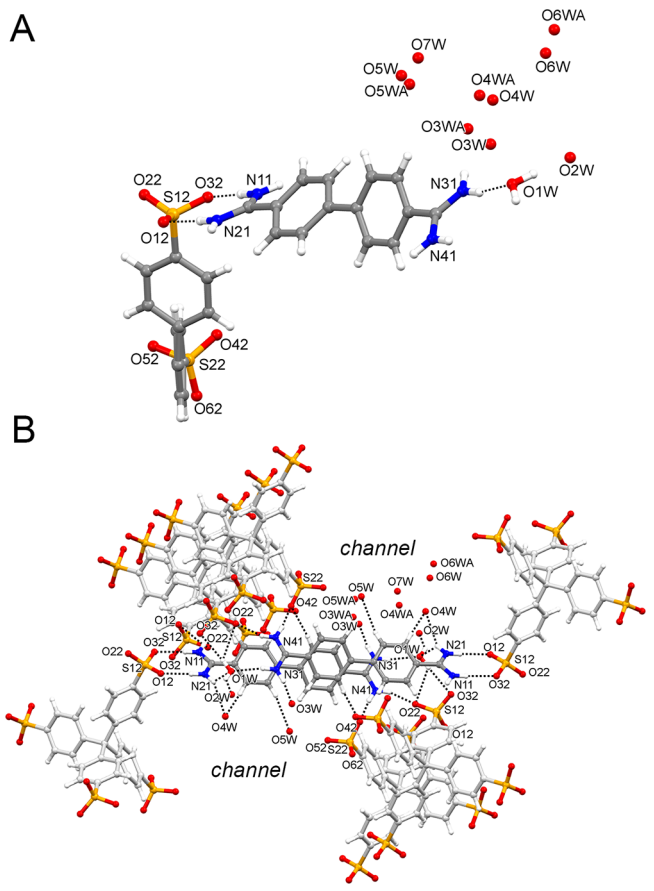

Figure 2. Molecular structure of **2**. (A) Asymmetric unit. (B) Highlight of the interactions exchanged by the BPAM cations.

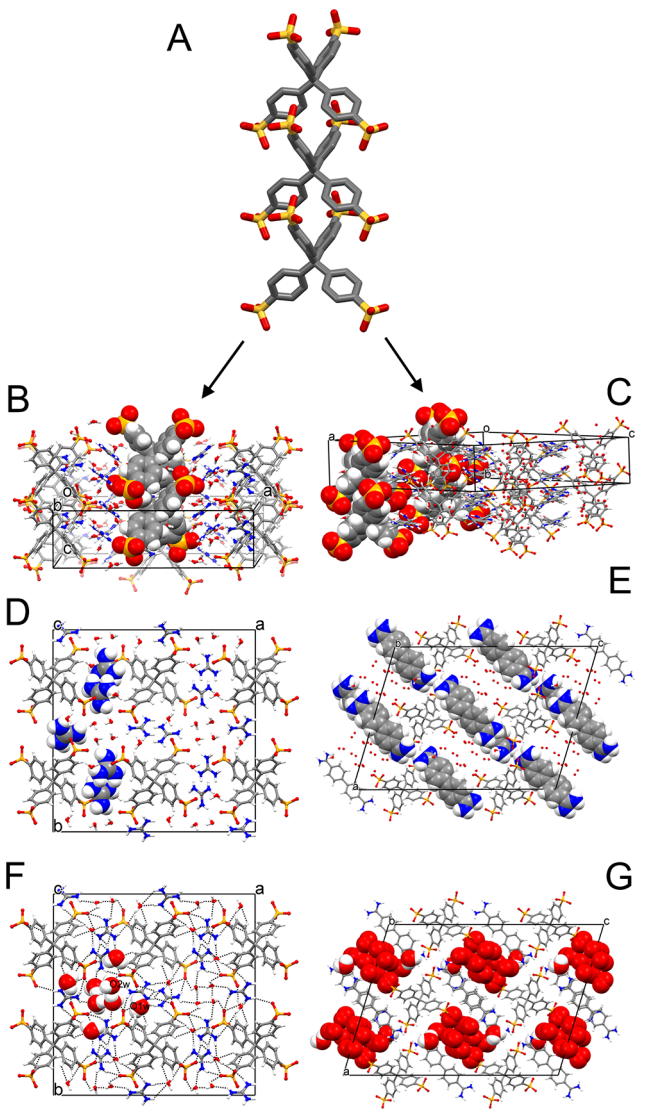

Figure 3. (A) Crystal packing of TFMS in **1** and **2**. Crystal packing of **1** (B, D, and F) and **2** (C, E, and G). Three compartments can be ideally identified in the lattice: one corresponds to the pillars formed by stacked TFMS anions (A–C), the second corresponds to the partially overlaid GN (D) and BPAM (E) cations, while the third is associated with the water molecules located in the channel-like cavity (F and G).

components, namely, the sulfonated anions, the organo-cations, and solvent molecules, are approximately arranged in pillars. The TFMS anions are interlocked with the aromatic rings (Figure 3A), whereas the GN or BPAM cations form $\pi-\pi$ stacks, which are more regular for BPAM according to the presence of aromatic rings. Additionally, the solvent molecules are located in channels defined by the two charged components.

Modification of the central tetrahedral carbon atom with an adamantane moiety resulted in new compounds. In fact, by cocrystallizing TFAS with the organo-cations PAM and BPAM two compounds were obtained: $(PAM)_2(TFAS)\cdot 9H_2O$ (**3**) and $(BPAM)_2(TFAS)\cdot 6.4H_2O\cdot 3.6MeOH$ (**4**), Figures 4 and 5. The compounds **3** and **4** crystallize in the tetragonal space group $P4_2/n$ and in the triclinic $P\bar{1}$, respectively. For both compounds, the TFAS/cation stoichiometry of 1/2 was confirmed by ^1H NMR (see Supporting Information). In the case of **3**, the water content was in agreement with NMR results (nine molecules per anionic unit), while in **4** the ^1H NMR experiments indicated the presence of six water molecules and two methanol molecules, which are slightly fewer than those found by the structural analysis. The asymmetric unit of **3** comprises one Ph-SO_3^- group of TFAS, one-half PAM cation, and 2.25 water molecules. Each oxygen atom of the SO_3^- group acts as an HB acceptor: two oxygen atoms are directly linked to PAM cations, whereas the third oxygen atom interacts with symmetry related water molecules (O1w), Figure 4A. PAM acts as an HB donor with all its eight hydrogen atoms interacting with four symmetry related O1w water molecules and with four water molecules present in the lattice channels (O2w and O4w) (Figure 4B). O1w and PAM form a stack that runs parallel to the *c* axis (see Figure 6C below).

The molecular structure of **4** is inherently less symmetric than that of **3** since the compound crystallizes in the triclinic space group $P\bar{1}$. The asymmetric unit comprises a TFMS anion, two BPAM cations, and water/methanol solvent of crystallization, Figure 5. The anions do not form pillars as in **1**–**3**, but they form an interlocked dimer, which is surrounded by cations and solvent molecules, see Figure 5B. In this dimer, the two anions are approaching each other with the trigonal face, hence pointing two different −Ph-SO_3^- groups in opposite directions. This arrangement is different from the one found in **1**–**3**, where the anions are piled along the binary axis of the tetrahedron.

Anionic dimer interactions take place by means of HBs mediated by solvent molecules to form a supramolecular pillar

DOI: 10.1021/acs.cgd.7b01538
Cryst. Growth Des. XXXX, XXX, XXX−XXX

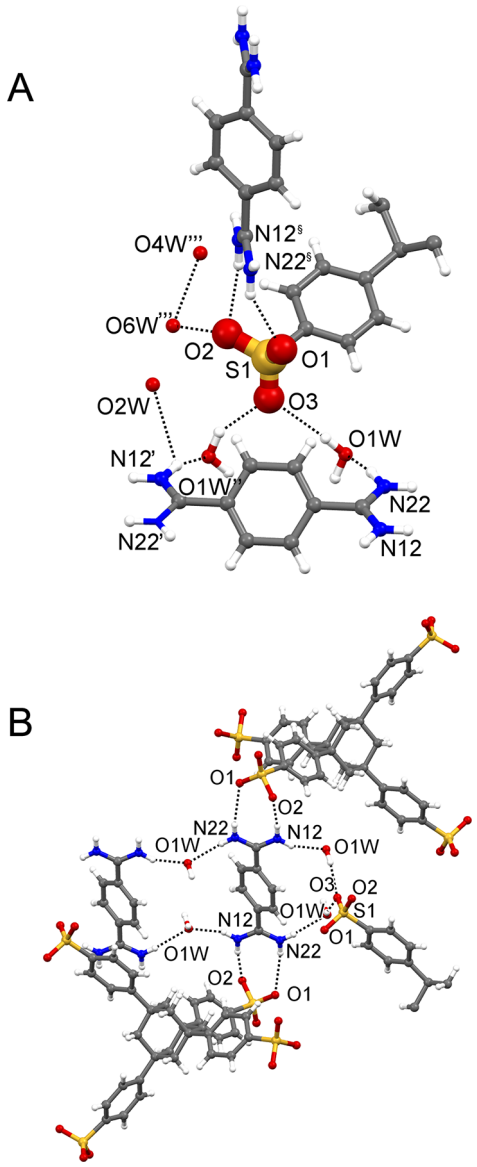

Figure 4. Molecular structure of **3**. (A) Highlight of the interactions exchanged by the sulfonate group with the surrounding cations and water molecules. (B) Interactions exchanged by the PAM cation. Symmetry codes: $' = 1 - x; 1 - y; 2 - z$, $'' = 1 - x; 1 - y; 1 - z$, $''' = 1 - y; 1/2 + x; z - 1/2$, $^{\S} = y; 3/2 - x; 3/2 - z$.

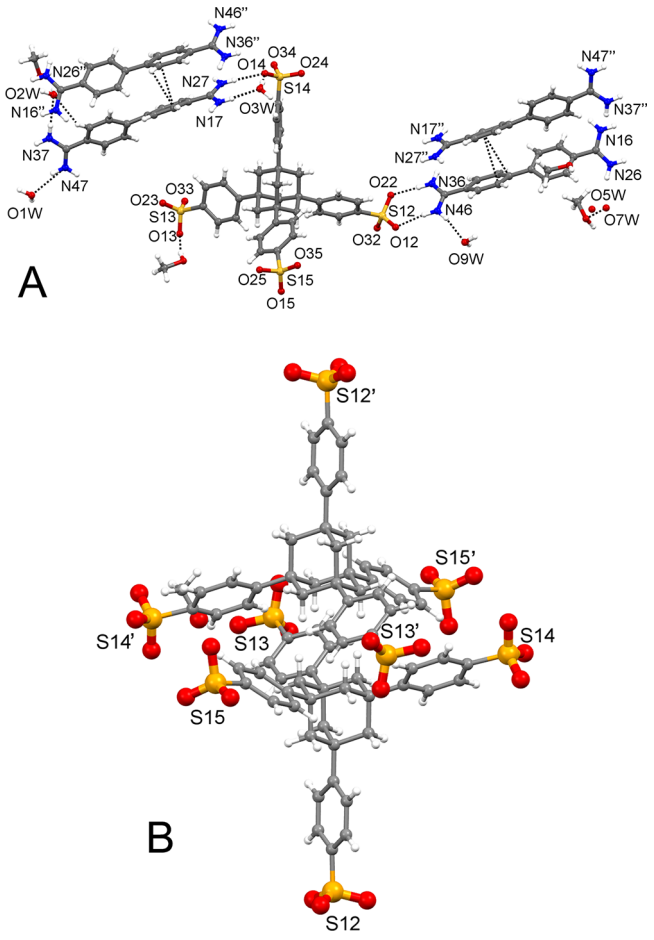

Figure 5. (A) Molecular structure of **4** and (B) the anionic dimer. Symmetry codes: $' = -x; -y; -z$, $'' = -x; 1 - y; 1 - z$.

that runs parallel to the *a* crystallographic axis (Figure 6B). Also the BPAM cations form dimers by means of a partial π stack that involves one of the two phenyl residues (Figure 5A). The BPAM dimers surround the anionic supramolecular chain, thus delimiting a channel occupied by solvent molecules that runs parallel to the [111] direction (Figure 6F). Interestingly, the crystal packing of **3** reveals considerable similarities to that of **1** and **2**. In fact, though the TFAS anions are larger than TFMS (in line with the presence of the adamantane unit instead of a single carbon atom), they are, like TFMS, interlocked, forming anionic pillars. The PAM cations alternate with water molecules (O1w) to form columnar stacks. Each cation exchanges four HBs with symmetry related O1w within the pillar, whereas in the direction perpendicular to the pillar axes, it interacts with two distinct sulfonate groups (Figure 6C).

The molecular structures of CXS and GN are reported in the literature.[58] For comparison purposes we report the structure of $(GN)_4CXS{\cdot}3H_2O$, which is the system that contains only water as the crystallization solvent. The asymmetric unit comprises a CXS anion, and four GN cations and three water molecules (Figure 7). The crystal packing shows the presence of puckered layers of calixarenes that are interposed between double layers of GN cations (Figure 7B). Of the three water molecules of crystallization, one is located inside the CXS cavity, whereas the remaining two serve as connectors between the CXS and GN components.

Let us now focus on the CXS/PAM (**5**) and CXS/BPAM systems (**6**). The asymmetric unit of **5** comprises one CXS moiety, a PAM cation, two half PAM cations, four water molecules, and half a methanol molecule of crystallization, giving rise to the molecular structure $(PAM)_2CXS{\cdot}4H_2O{\cdot}1/2MeOH$. The ^1H NMR confirmed the 1/2 anion/cation ratio and the presence of methanol, even though the methanol quantification was hampered by the presence of peaks partially overlapping those of the water molecules. All of the sulfonate groups act as HB acceptors toward $-NH_2$ groups of PAM and water molecules. One PAM cation is located above the calix cavity, exchanging four direct HB interactions with the sulfonate oxygens surrounding the cavity, a HB with a sulfonate group of an adjacent calixarene, and three HBs with water molecules acting as bridges with vicinal anions and cations (Figure 8A).

The CXS upper rim unit is surrounded by six-symmetry related PAM cations that interact with the sulfonates by means of HBs. The PAM cations located outside the CXS upper rim

DOI: 10.1021/acs.cgd.7b01538
Cryst. Growth Des. XXXX, XXX, XXX−XXX

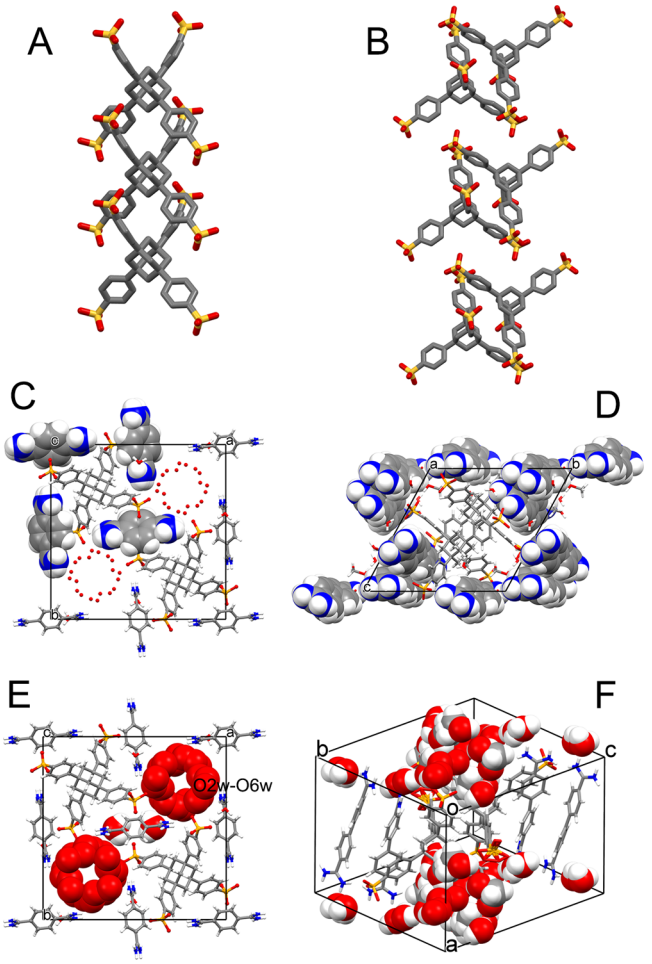

Figure 6. Crystal packing of **3** and **4**. (A) Pillars formed by stacked TFMS anions in **3**. (B) Pillars formed by stacked TFMS dimers in **4**. (C) PAM-water stacks in **3**, (D) BPAM dimers in **4**. Channels occupied by water molecules in **3** (E) and in **4** (F).

link vicinal CSX moieties, favoring the formation of puckered cationic/anionic layers (Figure 8B–C and Figure 9A–B). Within these ideal layers, the CXS anions are oriented in opposite directions (Figure 8C). The water molecules of crystallization occupy channels delimited by SO_3^- and phenyl rings of CXS and by NH_2 moieties of PAM. These channels run parallel to the *b* crystallographic axis (Figure 9C).

The molecular structure of **6** is reported in Figure 10. The asymmetric unit comprises half a calixarene moiety, one BPAM cation, two half methanol molecules, and four water molecules of crystallization: the overall formula unit corresponds to $(BPAM)_2(CXS)\cdot 8H_2O\cdot 2CH_3OH$. One methanol molecule is located in the CXS cavity, exchanging CH$\cdots\pi$ interactions with the methyl group and the phenyl rings surrounding the cavity. The hydroxyl group acts as HB donor with the O(41) atom of a sulfonate residue. Given the CXS symmetry, the methanol molecule is statically disordered in two positions related by a binary crystallographic axis.

The upper rim of the CXS moiety interacts with BPAM cations and water molecules (O1w, O2w, and O3w) through an extensive net of HBs, whereas a water molecule of crystallization (O4w) and a methanol molecule are located close to the lower rim. The aromatic sides of the CXS are involved in two different interactions with the surrounding molecules. The $\pi-\pi$ interactions determine the formation of

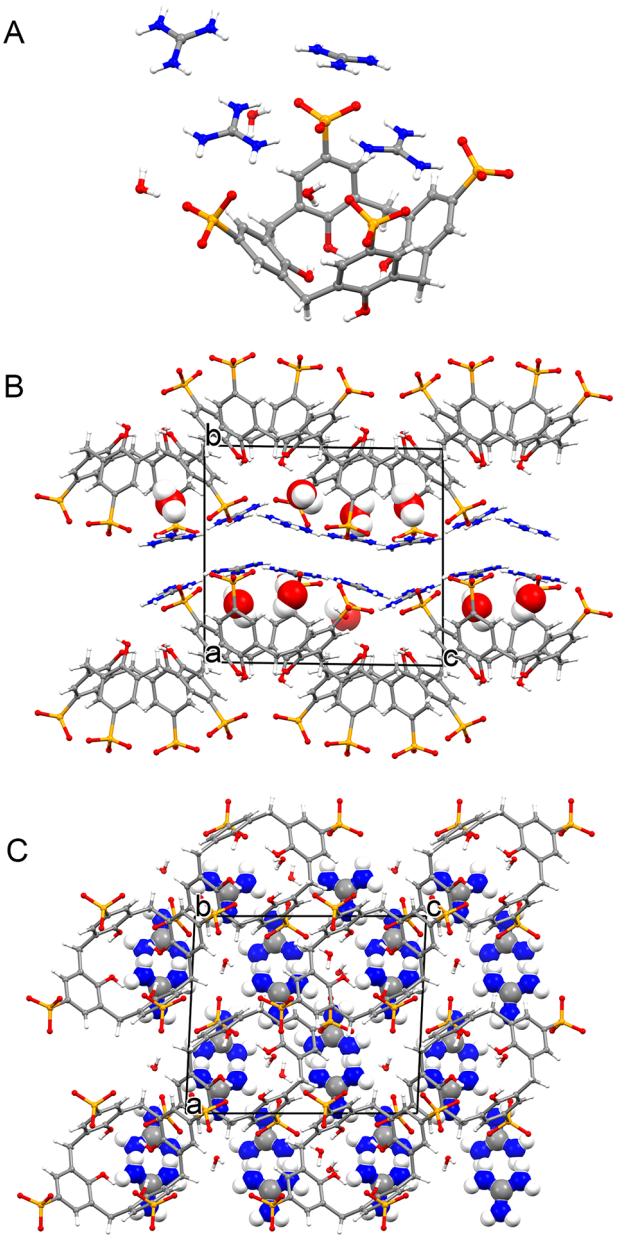

Figure 7. Molecular structure of $(GN)_4CXS\cdot 3H_2O$. (A) Asymmetric unit, (B) crystal packing projected along the *a* axis, (C) crystal packing projected along the *b* axis.[58]

supramolecular chains that run parallel to the *c* crystallographic axis (the distance between the aromatic planes is approximately 3.55 Å). Within these chains, the CXS moieties are oriented in opposite fashion (Figure 10D). Likewise, the BPAM cations form irregular stacks parallel to the *c* axis that are interposed between the CXS chains. As a result, CSX/BPAM mixed supramolecular layers are formed, which are parallel to the *ac* crystallographic plane. The water molecules are located between these layers acting as HB linkers (Figure 10C).

Hydration Analysis. A common feature of all the supramolecular architectures here reported is the double role played by the water molecules: one fraction acts directly to form HB bridges between the anions and cations, while the other lies in the channels (**1**–**4**) or in the more confined cavities (**5** and **6**). In compound **1** the volume occupied by water molecule was calculated to be 14% of the unit cell

DOI: 10.1021/acs.cgd.7b01538
Cryst. Growth Des. XXXX, XXX, XXX–XXX

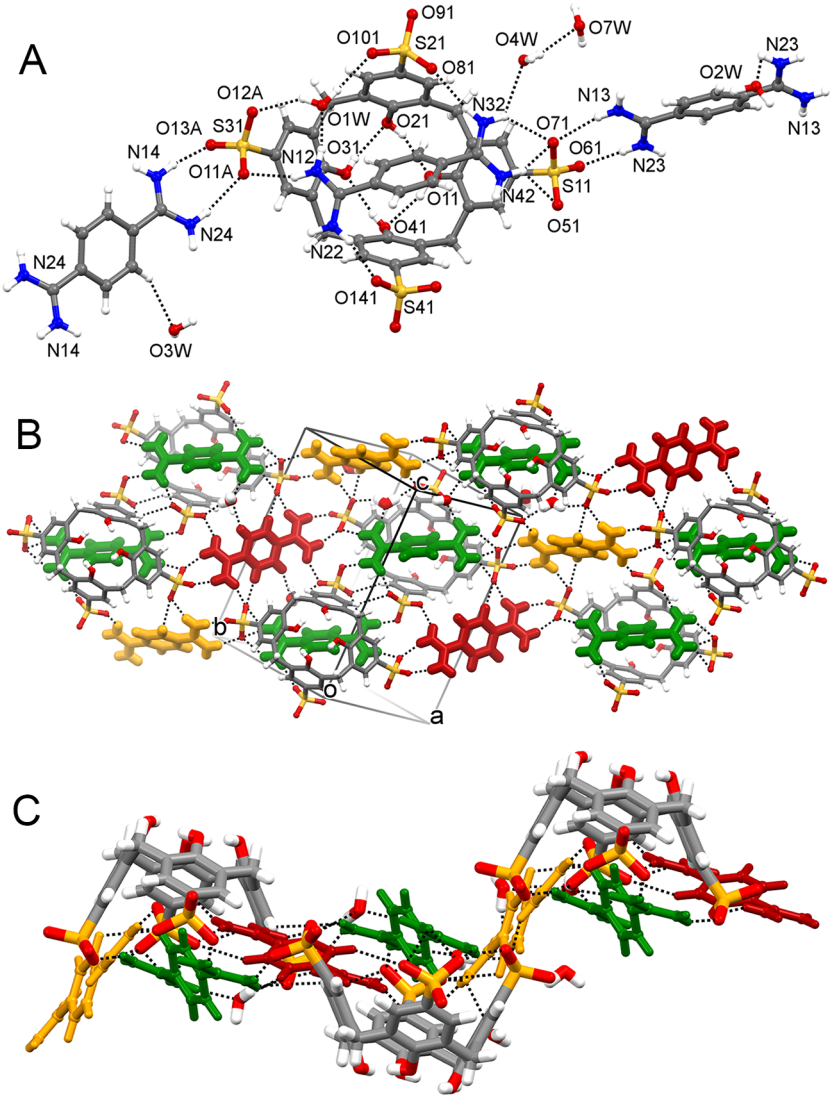

Figure 8. (A) Molecular structure of **5**. (B) Network of the HBs exchanged by the cations and anions in the cationic/anionic layer. (C) Side view of the puckered layer of cation and anion plane. In B and C, the three different types of PAM cations contained in the asymmetric unit are depicted in green, red, and yellow, respectively.

volume, while in compound **2** the bulkier cationic BPAM favored the formation of larger cavities and a larger water occupancy of the unit cell volume (25%) (Figure 11).[52] The DSC analysis of compound **1** revealed the presence of different water molecule types that are easily discriminated according to the position of the thermogram peaks (Figure S1, Supporting Information). In fact, the low temperature peaks (at about 80 °C) pertain to the removal of loosely bound water (O2w in the channel), whereas higher temperature peaks are associated with the loss of strongly bound water (O1w). In compound **2**, most of the water molecules occupy a channel-like cavity that lies parallel to the *b* crystallographic axis. In the DSC thermogram, a deep broad endothermic peak appears at 80 °C and can be assigned to channel water, which is potentially easy to remove. The peaks above 100 °C could correspond to water molecules H-bonded with the cation−anion assembly.

The volume occupied by water molecules in **3** and by solvent molecules (water and methanol) in **4** corresponds approximately to 20% of the unit cell volume. In both compounds, two different water molecules are present. In **3** the disordered water molecules (O2w−O6w) occupy a channel-like cavity, which runs parallel to the *c* crystallographic axis, and the O1w water molecule acts as HBs-acceptor with the PAM cation and as HB-donor with two symmetry related sulfonate groups linking the anions in the *ab* plane. In the DSC profile, two endothermic peaks are present: one peak at 94 °C that can be assigned to the water molecules in the channels and a smaller peak at 116 °C associated with structural water. In **4**, the DSC analysis shows a larger broad peak at 94 °C, corresponding to solvent molecules arranged in the channel-like cavities. The volume occupied by solvent molecules in **5** and **6** corresponds to approximately 12% of the unit cell volume (Figure 11). The relatively small water content can be due to the different symmetry of the CSX unit, with respect to the TFMS and TFAS anions. In fact, CXS exhibits only one main direction according to which it can act as HB acceptor, namely, the upper rim of the calixarene where the sulfonate groups are located. Differently, the symmetry of TFMS and TFAS projects the HB interactions along a divergent tetrahedral geometry suitable for larger cavity formation. In addition, the CXS symmetry favors the formation of $\pi-\pi$ stacks among different calixarene units or PAM and BPAM cations, whereas TFMS and TFAS have the

DOI: 10.1021/acs.cgd.7b01538
Cryst. Growth Des. XXXX, XXX, XXX−XXX

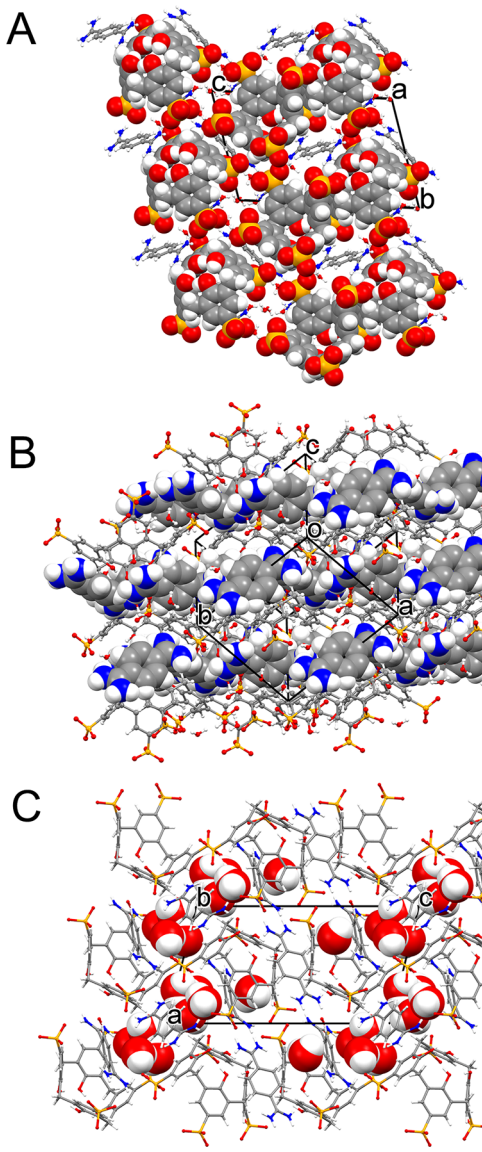

Figure 9. Crystal packing of **5**: CXS anions (A), PAM cations (B), and channels occupied by water molecules (C).

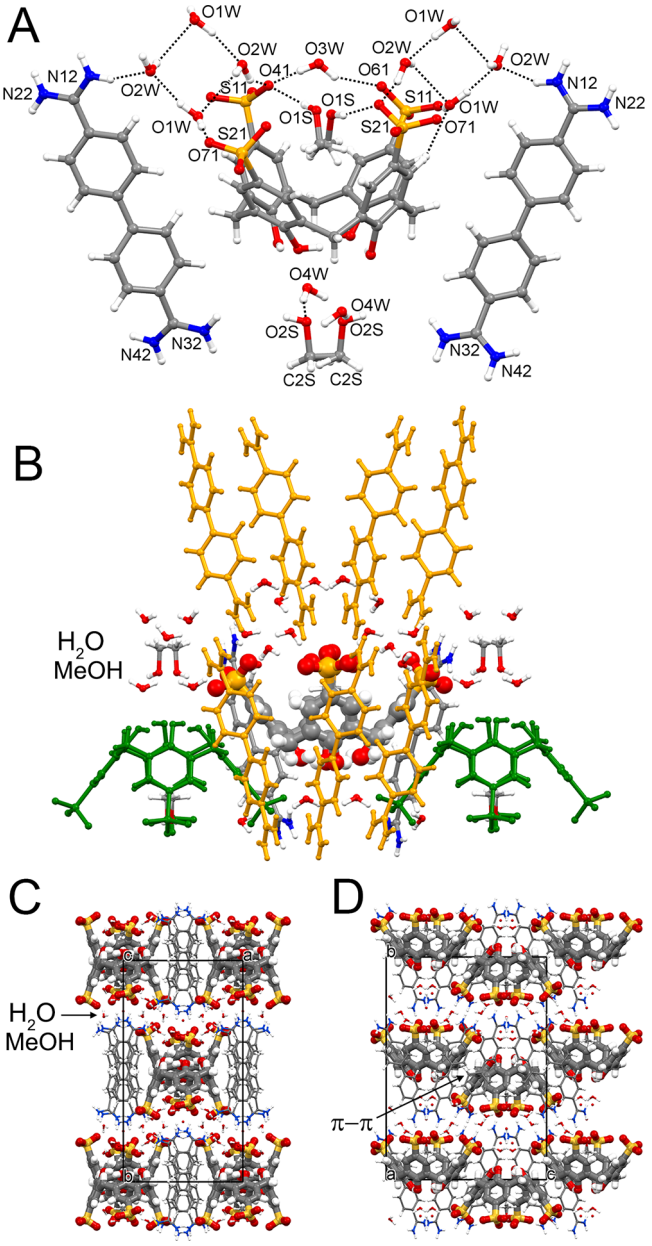

Figure 10. Molecular structure of **6**: (A) network of the HBs exchanged by the cations, anions and solvent molecules. (B) Lattice environment surrounding a CXS unit: the symmetry-related CXS and BPAM cations are depicted in green and orange, respectively. Symmetry codes are not indicated for clarity. Crystal packing of **6**: solvent molecules are located between cation/anion layers (C); highlight of the π- π stack between symmetry related CXS (D).

tendency to form interlocked columnar molecular arrangements, which are more apt to give rise to channel-like cavities. In fact, in **5** and **6** the solvent molecules are located in more defined cavities (as in **5**) or in layers (as in **6**). The DSC analysis of **5** shows a broad peak at 65 °C, which can be associated with the loss of the methanol, as observed by X-ray and NMR analyses. The peaks at 102 °C presumably correspond to water molecules, which are bound to the cation−anion framework and H-bonded to other water molecules. Instead, for compound **6**, the broad peak centered at about 76 °C may correspond to the methanol molecules present in the CXS cavity and close to the CXS lower rim, as well as to the loosely bound water molecules lodged in the layers of the molecular building.

CONCLUSIONS

The construction of crystal lattices by tetrafunctional anions, that protrude in 3D in different directions and mono- or divalent organic cations, leads to intriguing architectures. In such structures, the role played by water confirms the tendency of multicharged or polar molecules to associate as hydrates.[37] Indeed, water plays a double role in the lattices: (1) it acts as a strut itself and (2) behaves as a guest in structural channels/cavities. The relevant role assumed by water, which in many cases is elusive to structural characterization, was successfully identified by single-crystal XRD analysis. The description of complex structures among densely charged organic molecules and the interplay of "pronubial" small molecules of water is relevant to the construction of new hydrates with enhanced solubility and the perspective to build cocrystals. The high number of charges and their directional distribution over the molecular surface result in new properties and enhance the

DOI: 10.1021/acs.cgd.7b01538
Cryst. Growth Des. XXXX, XXX, XXX−XXX

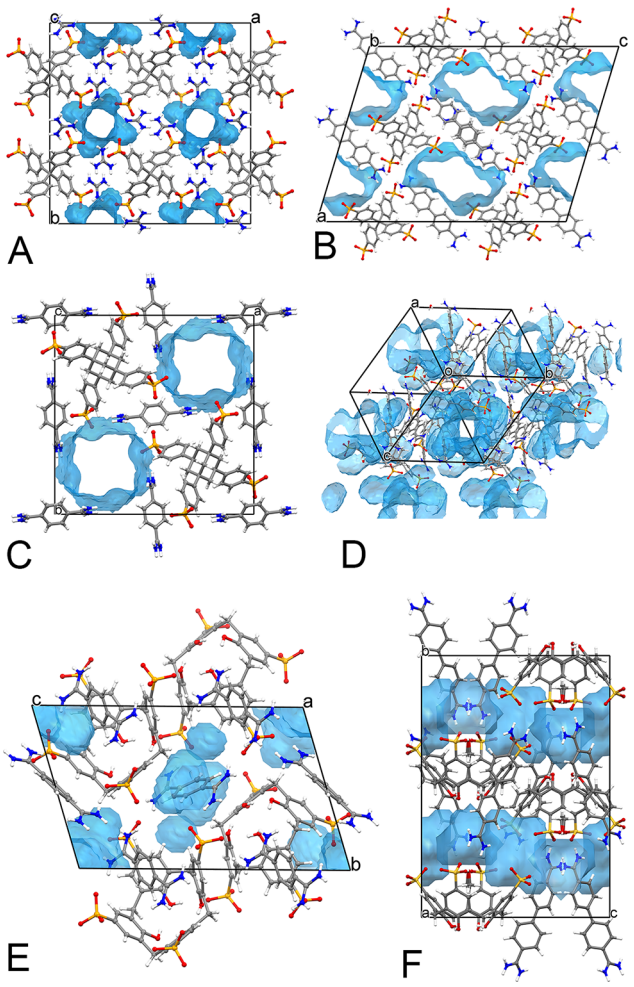

Figure 11. Crystal packing of **1** (A), **2** (B), **3** (C), **4** (D), **5** (E), and **6** (F) showing the volume occupied by water or solvent molecules.

potential of the crystallization processes, which is of great relevance in applicative fields where control over the crystallization process is fundamentally of great importance.

■ ASSOCIATED CONTENT

Supporting Information

The Supporting Information is available free of charge on the ACS Publications website at DOI: 10.1021/acs.cgd.7b01538.

DSC and TGA plots, ^{1}H NMR spectra, FT-IR spectra, crystal data, PXRD spectra (PDF)

Accession Codes

CCDC 1573468−1573473 contain the supplementary crystallographic data for this paper. These data can be obtained free of charge via www.ccdc.cam.ac.uk/data_request/cif, or by emailing data_request@ccdc.cam.ac.uk, or by contacting The Cambridge Crystallographic Data Centre, 12 Union Road, Cambridge CB2 1EZ, UK; fax: +44 1223 336033.

■ AUTHOR INFORMATION

Corresponding Authors

*(L.M.) E-mail: luciano.marchio@unipr.it.
*(A.C.) E-mail: angiolina.comotti@unimib.it.
*(T.B.) E-mail: tben@jlu.edu.cn.

ORCID

Teng Ben: 0000-0002-0847-330X
Luciano Marchio: 0000-0002-0025-1104
Angiolina Comotti: 0000-0002-8396-8951

Funding

A.C. would like to thank Cariplo Foundation 2016, PRIN 2016-NAZ-0104, and INSTM-RL14−2016 for financial support.

Notes

The authors declare no competing financial interest.

■ ACKNOWLEDGMENTS

Elettra synchrotron facility (XRD1) is acknowledged for providing support for some of the X-ray data collections. Chiesi Farmaceutici Spa is acknowledged for their support for the X-ray equipment. The COST action CM1402 “Crystallize” is acknowledged for networking support.

■ REFERENCES

(1) Etter, M. C. Hydrogen bonds as design elements in organic chemistry. *J. Phys. Chem.* **1991**, *95*, 4601−4610.
(2) Steiner, T. The hydrogen bond in the solid state. *Angew. Chem., Int. Ed.* **2002**, *41*, 48−76.
(3) Prins, L. J.; Reinhoudt, D. N.; Timmerman, P. Noncovalent synthesis using hydrogen bonding. *Angew. Chem., Int. Ed.* **2001**, *40*, 2382−2426.
(4) Zerkowski, J. A.; Seto, C. T.; Wierda, D. A.; Whitesides, G. M. The design of organic structures in the solid state: hydrogen-bonded molecular “tapes”. *J. Am. Chem. Soc.* **1990**, *112*, 9025−9026.
(5) Gilli, P.; Gilli, G. In *Strength from Weakness: Structural Consequences of Weak Interactions in Molecules, Supermolecules, and Crystals*; Domenicano, A., Hargittai, I., Eds.; Springer: Netherlands: Dordrecht, 2002; pp 261−280.
(6) Spackman, M. A.; McKinnon, J. J. Fingerprinting intermolecular interactions in molecular crystals. *CrystEngComm* **2002**, *4*, 378−392.
(7) Lehn, J. M. *Supramolecular Chemistry: Concept and Perspectives*; VCH: Weinheim Interaction, 1995.
(8) Aakeröy, C. B. Crystal engineering: strategies and architectures. *Acta Crystallogr., Sect. B: Struct. Sci.* **1997**, *53*, 569−586.
(9) Weber, E.; Aoyama, Y.; Caira, M. R.; Desiraju, G. R.; Glusher, J. P.; Hamilton, A. D.; Melèndez, R. E.; Namgia, A. *Design of Organic Solids*; Weber, E., Ed.; Springer-Verlag: Berlin, 1998.
(10) Seth, M.; Singh, M.; Jana, D.; Choudhury, K.; Mukhopadhyay, K.; Manna, P.; Mitra, M.; Das, A.; Kar, T.; Kim, K. S. Molecular architecture using novel types of non-covalent π-interactions involving aromatic neutrals, aromatic cations and π-anions. *CrystEngComm* **2013**, *15*, 1285−1288.
(11) Manna, P.; Seth, S. K.; Mitra, M.; Das, A.; Singh, N. J.; Choudhury, S. R.; Kar, T.; Mukhopadhyay, S. A successive layer-by-layer assembly of supramolecular frameworks driven by a novel type of face-to-face π^+−π^+ interactions. *CrystEngComm* **2013**, *15*, 7879−7886.
(12) Manna, P.; Seth, S. K.; Bauzá, A.; Mitra, M.; Choudhury, S. R.; Frontera, A.; Mukhopadhyay, S. pH dependent formation of unprecedented water−bromide cluster in the bromide salts of PTP assisted by anion− π interactions: synthesis, structure, and DFT Study. *Cryst. Growth Des.* **2014**, *14*, 747−755.
(13) Manna, P.; Seth, S. K.; Mitra, M.; Choudhury, S. R.; Bauzá, A.; Frontera, A.; Mukhopadhyay, S. Experimental and computational study of counterintuitive $ClO_4^-\cdots ClO_4^-$ interactions and the interplay between π^+−π and Anion$\cdots\pi^+$ interactions. *Cryst. Growth Des.* **2014**, *14*, 5812−5821.
(14) Qureshi, N.; Yufit, D. S.; Steed, K. M.; Howard, J. A. K.; Steed, J. W. Hydrogen bonding effects in anion binding calixarenes. *CrystEngComm* **2014**, *16*, 8413−8420.
(15) Edkins, R. M.; Hayden, E.; Steed, J. W.; Fucke, K. Conserved hydrogen bonding in tetrahydrocarbazolone derivatives: influence of solution-state assembly on crystal form nucleation. *Chem. Commun.* **2015**, *51*, 5314−5317.

DOI: 10.1021/acs.cgd.7b01538
Cryst. Growth Des. XXXX, XXX, XXX−XXX

(16) Qureshi, N.; Yufit, D. S.; Steed, K. M.; Howard, J. A. K.; Steed, J. W. Anion hydrogen bonding from a 'revealed' urea ligand. *CrystEngComm* **2016**, *18*, 5333−5337.
(17) Soegiarto, A. C.; Comotti, A.; Ward, M. D. Controlled orientation of polyconjugated guest molecules in tunable host cavities. *J. Am. Chem. Soc.* **2010**, *132*, 14603−14616.
(18) Liu, Y.; Xiao, W.; Yi, J. J.; Hu, C.; Park, S. J.; Ward, M. D. Regulating the Architectures of Hydrogen-Bonded Frameworks through Topological Enforcement. *J. Am. Chem. Soc.* **2015**, *137*, 3386−3392.
(19) Ermer, O.; Eling, A. Distorted Triple-Diamond Structure of 3, 3-Bis (carboxymethyl) glutaric Acid ("Methanetetraacetic Acid"). *Angew. Chem., Int. Ed. Engl.* **1988**, *27*, 829−833.
(20) Ermer, O. Five-fold diamond structure of adamantane-1, 3, 5, 7-tetracarboxylic acid. *J. Am. Chem. Soc.* **1988**, *110*, 3747−3754.
(21) Sun, Y.; Sun, Y.; Zheng, H.; Wang, H.; Han, Y.; Yang, Y.; Wang, L. Four calcium(II) coordination polymers based on 2,5-dibromoterephthalic acid and different N-donor organic species: syntheses, structures, topologies, and luminescence properties. *CrystEngComm* **2016**, *18*, 8664−8671.
(22) Xiao, Z.; Wang, W.; Xue, R.; Zhao, L.; Wang, L.; Zhang, Y. Trimer formation of 6-methyl-1, 3, 5-triazine-2, 4-diamine in salt with organic and inorganic acids: analysis of supramolecular architecture. *Sci. China: Chem.* **2014**, *57*, 1731−1737.
(23) Wang, L.; Xue, R.; Li, Y.; Zhao, Y.; Liu, F.; Huang, K. Hydrogen-bonding patterns in a series of multi-component molecular solids formed by 2,3,5,6-tetramethylpyrazine with selected carboxylic acids. *CrystEngComm* **2014**, *16*, 7074−7089.
(24) Pang, Y.; Xing, P.; Geng, X.; Zhu, Y.; Liu, F.; Wang, L. Supramolecular assemblies of 2-hydroxy-3-naphthoic acid and N-heterocycles via various strong hydrogen bonds and weak X···π (X═C−H, π) interactions. *RSC Adv.* **2015**, *5*, 40912−40923.
(25) Yamamoto, A.; Uehara, S.; Hamada, T.; Miyata, M.; Hisaki, I.; Tohnai, N. Diamondoid porous organic salts toward applicable strategy for construction of versatile porous structures. *Cryst. Growth Des.* **2012**, *12*, 4600−4606.
(26) Yamamoto, A.; Hamada, T.; Hisaki, I.; Miyata, M.; Tohnai, N. Dynamically Deformable Cube-like Hydrogen-Bonding Networks in Water-Responsive Diamondoid Porous Organic Salts. *Angew. Chem., Int. Ed.* **2013**, *52*, 1709−1712.
(27) Holman, K. T.; Pivovar, A. M.; Swift, J. A.; Ward, M. D. Metric engineering of soft molecular host frameworks. *Acc. Chem. Res.* **2001**, *34*, 107−118.
(28) Liu, Y.; Hu, C.; Comotti, A.; Ward, M. D. Supramolecular Archimedean cages assembled with 72 hydrogen bonds. *Science* **2011**, *333*, 436−441.
(29) Ilioudis, C. A.; Bearpark, M. J.; Steed, J. W. Hydrogen bonds between ammonium ions and aromatic rings exist and have key consequences on solid-state and solution phase properties. *New J. Chem.* **2005**, *29*, 64−67.
(30) Fucke, K.; Anderson, K. M.; Filby, M. H.; Henry, M.; Wright, J.; Mason, S. A.; Gutmann, M. J.; Barbour, L. J.; Oliver, C.; Coleman, A. W.; Atwood, J. L.; Howard, J. A. K.; Steed, J. W. The Structure of Water in p-Sulfonatocalix [4] arene. *Chem. - Eur. J.* **2011**, *17*, 10259−10271.
(31) Sheng, Y.; Chen, Q.; Yao, J.; Lu, Y.; Liu, H.; Dai, S. Guest-Induced Breathing Effect in a Flexible Molecular Crystal. *Angew. Chem., Int. Ed.* **2016**, *55*, 3378−3381.
(32) Yamamoto, A.; Hirukawa, T.; Hisaki, I.; Miyata, M.; Tohnai, N. Multifunctionalized porosity in zeolitic diamondoid porous organic salt: selective adsorption and guest-responsive fluorescent properties. *Tetrahedron Lett.* **2013**, *54*, 1268−1273.
(33) Desiraju, G. R. Supramolecular synthons in crystal engineering—a new organic synthesis. *Angew. Chem., Int. Ed. Engl.* **1995**, *34*, 2311−2327.
(34) Desiraju, G. R. Crystal engineering: from molecule to crystal. *J. Am. Chem. Soc.* **2013**, *135*, 9952−9967.
(35) Thakur, T. S.; Dubey, R.; Desiraju, G. R. Crystal structure and prediction. *Annu. Rev. Phys. Chem.* **2015**, *66*, 21−42.
(36) Desiraju, G. R. Hydration in organic crystals: prediction from molecular structure. *J. Chem. Soc., Chem. Commun.* **1991**, *6*, 426−428.
(37) Infantes, L.; Fabian, L.; Motherwell, W. D. S. Organic crystal hydrates: what are the important factors for formation. *CrystEngComm* **2007**, *9*, 65−71.
(38) Infantes, L.; Chisholm, J.; Motherwell, S. Extended motifs from water and chemical functional groups in organic molecular crystals. *CrystEngComm* **2003**, *5*, 480−486.
(39) Varughese, S.; Desiraju, G. R. Using water as a design element in crystal engineering. Host− guest compounds of hydrated 3, 5-dihydroxybenzoic acid. *Cryst. Growth Des.* **2010**, *10*, 4184−4196.
(40) Sansam, B. C. R.; Anderson, K. M.; Steed, J. W. A simple strategy for crystal engineering water clusters. *Cryst. Growth Des.* **2007**, *7*, 2649−2653.
(41) Sander, J. R. G.; Bučar, D.-K.; Henry, R. F.; Giangiorgi, B. N.; Zhang, G. G. Z.; MacGillivray, L. R. 'Masked synthons' in crystal engineering: insulated components in acetaminophen cocrystal hydrates. *CrystEngComm* **2013**, *15*, 4816−4822.
(42) Khankari, R. K.; Grant, D. J. W. Pharmaceutical hydrates. *Thermochim. Acta* **1995**, *248*, 61−79.
(43) Karki, S.; Friščić, T.; Jones, W.; Motherwell, W. D. S. Screening for pharmaceutical cocrystal hydrates via neat and liquid-assisted grinding. *Mol. Pharmaceutics* **2007**, *4*, 347−354.
(44) Mascal, M.; Infantes, L.; Chisholm, J. Water oligomers in crystal hydrates—what's news and what isn't? *Angew. Chem., Int. Ed.* **2006**, *45*, 32−36.
(45) Sarma, B.; Nangia, A. Tetrakis (4-sulfophenyl) methane dodecahydrate. Reversible and selective water inclusion and release in an organic host. *CrystEngComm* **2007**, *9*, 628−631.
(46) Hoffart, D. J.; Côté, A. P.; Shimizu, G. K. H. An adamantane-based coordination framework with the first observation of discrete metal sulfonate clusters. *Inorg. Chem.* **2003**, *42*, 8603−8605.
(47) Song, G.; Zhu, H.; Chen, L.; Liu, S.; Luo, Z. Novel Disubstituted Phenylene-Linked Bis-imidazole Derivatives: Facile Synthesis and Optical Properties. *Helv. Chim. Acta* **2010**, *93*, 2397−2405.
(48) Ismail, M. A.; Arafa, R. K.; Brun, R.; Wenzler, T.; Miao, Y.; Wilson, W. D.; Generaux, C.; Bridges, A.; Hall, J. E.; Boykin, D. W. Synthesis, DNA affinity, and antiprotozoal activity of linear dications: terphenyl diamidines and analogues. *J. Med. Chem.* **2006**, *49*, 5324−5332.
(49) Bruker AXS: Madison, WI, 1994.
(50) Siemens Industrial Automation, I: Madison, WI, 1996.
(51) Lausi, A.; Polentarutti, M.; Onesti, S.; Plaisier, J. R.; Busetto, E.; Bais, G.; Barba, L.; Cassetta, A.; Campi, G.; Lamba, D.; Pifferi, A.; Mande, S. C.; Sarma, D. D.; Sharma, S. M.; Paolucci, G. Status of the crystallography beamlines at Elettra. *Eur. Phys. J. Plus* **2015**, *130*, 1−8.
(52) Kabsch, W. Integration, scaling, space-group assignment and post-refinement. *Acta Crystallogr., Sect. D: Biol. Crystallogr.* **2010**, *66*, 125−132.
(53) Winn, M. D.; Ballard, C. C.; Cowtan, K. D.; Dodson, E. J.; Emsley, P.; Evans, P. R.; Keegan, R. M.; Krissinel, E. B.; Leslie, A. G. W.; McCoy, A.; McNicholas, S. J.; Murshudov, G. N.; Pannu, N. S.; Potterton, E. A.; Powell, H. R.; Read, R. J.; Vagin, A.; Wilson, K. S. Overview of the CCP4 suite and current developments. *Acta Crystallogr., Sect. D: Biol. Crystallogr.* **2011**, *67*, 235−242.
(54) Evans, P. R.; Murshudov, G. N. How good are my data and what is the resolution? *Acta Crystallogr., Sect. D: Biol. Crystallogr.* **2013**, *69*, 1204−1214.
(55) Sheldrick, G. M. SHELXT−Integrated space-group and crystal-structure determination. *Acta Crystallogr., Sect. A: Found. Adv.* **2015**, *71*, 3−8.
(56) Sheldrick, G. M. Crystal structure refinement with SHELXL. *Acta Crystallogr., Sect. C: Struct. Chem.* **2015**, *71*, 3−8.
(57) Macrae, C. F.; Edgington, P. R.; McCabe, P.; Pidcock, E.; Shields, G. P.; Taylor, R.; Towler, M.; van de Streek, J. Mercury: visualization and analysis of crystal structures. *J. Appl. Crystallogr.* **2006**, *39*, 453−457.

DOI: 10.1021/acs.cgd.7b01538
Cryst. Growth Des. XXXX, XXX, XXX−XXX

(58) Liu, Y.; Ward, M. D. Molecular capsules in modular frameworks. *Cryst. Growth Des.* **2009**, *9*, 3859−3861.
(59) Wood, P. A.; Olsson, T. S. G.; Cole, J. C.; Cottrell, S. J.; Feeder, N.; Galek, P. T. A.; Groom, C. R.; Pidcock, E. Evaluation of molecular crystal structures using Full Interaction Maps. *CrystEngComm* **2013**, *15*, 65−72.
(60) Estimated using a probe radius 1.2 Å and a space grid of 0.3 Å.

DOI: 10.1021/acs.cgd.7b01538
Cryst. Growth Des. XXXX, XXX, XXX−XXX